Structural and electronic characterization of Co nanostructures on Au(332)

ARTICLE *in* SURFACE SCIENCE · JULY 2013

Impact Factor: 1.93 · DOI: 10.1016/j.susc.2013.07.025

Surface Science 617 (2013) 87–93

Contents lists available at ScienceDirect

Surface Science

journal homepage: www.elsevier.com/locate/susc

Structural and electronic characterization of Co nanostructures on Au(332)

Mauricio J. Prieto *, Emilia A. Carbonio, Richard Landers, Abner de Siervo

Departamento de Física Aplicada, Instituto de Física Gleb Wataghin, Universidade Estadual de Campinas, 13083–859, Campinas, SP, Brazil

ARTICLE INFO

Article history:
Received 2 April 2013
Accepted 29 July 2013
Available online 3 August 2013

Keywords:
Nanoislands
Vicinal
Cobalt
Adsorption

ABSTRACT

Co nanoislands were grown on (332) vicinal surface of Au in UHV using the e-beam evaporation technique. Scanning tunneling microscopy results reveal that Co deposition occurs following an islanding mode for θ_{Co} ranging from 0.17 to 0.64 ML. At low coverage nanoislands show a monolayer height, while at higher Co loadings, islands have a maximum bilayer height. XPS measurements rule out the possibility of alloy formation provided that binding energy of Co2p core lines remains unchanged as cobalt loading increases. Also, XPS data reveals that, when subjected to thermal annealing, Co atoms diffuse into Au crystal retaining its chemical nature as before the annealing. Finally, NO adsorption experiments show that Co nanostructures are partially oxidized upon adsorption, as evidenced by changes in core photoemission lineshapes of the Co2p lines. Also, NO adsorption seems to inhibit Co atom diffusion into Au crystal during moderate thermal treatment.

1. Introduction

Nanostructures in general have been the subject of several investigations from many points of view over the last decades. The interest of society in such materials is based on the unique properties exhibited at the nanoscale. For instance, physicochemical properties that already exist in bulk materials can be abruptly enhanced as a consequence of confinement and, even more interesting, new properties may arise.

In general, transition metal nanoparticles (TMNP) have been extensively studied for several applications in many areas of research: catalysis, optics, magnetism, medicine, biochemistry, electronics, etc [1]. Two main factors can be related with the unique properties of TMNP, namely: electronic and geometric. Electronic factors may arise e.g. from the fact that, as a particle is sized down to the nanoscale, the size of valence band electron wave function starts to be comparable to the dimension of the nanoparticles. Consequently, the d-valence band width and centroid is drastically modified and very dependent on particle size and geometry, thus modifying the properties of the material. On the other hand the geometric factor arises from the fact that TMNP may adopt different geometries depending on their thermodynamic stability and the synthesis route adopted. For instance, different NP geometries of the same material may exhibit completely different surface atomic arrangement and hence, site geometry that will change the material's behavior. This fact is particularly important in catalysis, where different geometries can produce more active and selective surfaces for chemical reactions [2].

On the other hand, modified single crystalline surfaces of low Miller index have been used in the last decades as model surfaces to improve the understanding of the effects mentioned earlier in TMNP, since correlations between these two factors and surface atomic arrangement can be established. Alternatively, high Miller index surfaces, or vicinal surfaces, offer much more interesting possibilities since the role of defects can be studied in a controlled manner. A vicinal surface is one that has its normal deviated from a given low index plane by few degrees. As a result, these surfaces have a high concentration of defects such as steps and kinks, of well-defined crystallographic orientation.

Among TMs cobalt is an interesting metal to study since it is applied both in fundamental research and industrial applications in a variety of areas such as energy storage [3], super-alloys [4], catalysis [5], medicine [6] and magnetism [7]. The chemical state of Co may vary from its metallic to oxide forms, or even alloyed with other TMs. Particularly, the importance of the Co/Au(hkl) system has been extensively addressed in the literature by several authors [8,9]. It has been reported in the literature that in the case of Co deposited in UHV on Au (111), nanostructures grow in the so-called islanding mode, where right after the nucleation process starts, the growth of the nuclei occurs by the formation of a bilayer of Co atoms. Furthermore, even though there is a considerable lattice mismatch between bulk Co and Au (~14%), Voigtlander et al. [9] found Co deposition on Au(111) to be epitaxial with islands edges aligned along the [110] direction. Additionally, Morgestern et al. [10] have determined using STM measurements a bilayer island height of 0.43 nm and that formation of a Moiré lattice takes place on Co islands.

In this paper we show a detailed study of the electronic structure and surface morphology of Co nanostructures deposited on Au(332) surface. The Au(332) surface can be expressed as Au [5 (111) × (110)], where (111) and (110) are the terrace and the step orientation, respectively

* Corresponding author. Tel.: +55 19 35215393.
E-mail addresses: prietomauricio@gmail.com (M.J. Prieto), emiliacarbonio@gmail.com (E.A. Carbonio).

0039-6028/$ – see front matter © 2013 Elsevier B.V. All rights reserved.
http://dx.doi.org/10.1016/j.susc.2013.07.025

and 5 is the number of atoms constituting the terrace. Despite the (111) orientation of the terrace, this surface does not undergo the well-known ($22 \times \sqrt{3}$) reconstruction of the basal 111 plane due mainly to strains in the surface unit cell after reconstruction and its surface structure remains stable in a wide temperature range [11]. These properties make the Au(332) surface an interesting candidate in the study of the effect of steps on the nucleation of Co nanostructures at low θ_{Co}. Regarding vicinal surfaces of Au, many publications about Co/Au(788) can be found in the literature [12]. However, the (788) surface is well known to undergo a reconstruction perpendicular to the terrace due to the $22 \times \sqrt{3}$ reconstruction of the (111) plane, thus emerging two types of sites for nucleation and consequent growth (fcc and hcp) [13]. Conversely, the (332) surface does not reconstruct, thus representing a completely different scenario where no preferential nucleation along the terrace will occur, although its limited size may control size distribution.

2. Experimental section

2.1. Equipment

All experiments were carried out in an ultra-high vacuum (UHV) system. The chamber is equipped with LEED optics, an SPECS-Phoibus 150 hemispherical electron analyzer with nine-channeltron detection, an Ar ion gun for sputtering, a water cooled evaporator and a high precision two rotation axis manipulator, allowing sample transfer and heating up to 1200 K by electron bombardment. The setup operates in a base pressure better than 5×10^{-10} mbar regime during evaporation and measurements. The XPS experiments were performed using Al Kα line. Additionally, the sample could be transferred directly to an adjoining chamber equipped with an Aarhus 150 (SPECS) scanning tunneling microscope (STM) operating under UHV, available for STM measurements with a tungsten tip in constant current mode. The operating base pressure during image acquisition was always in the 10^{-11} mbar range and typical operating conditions were 0.15–0.3 nA of tunneling current and 1.2–1.75 V bias. ImageJ and WSxM software were used for image processing [14]. Co coverage (θ_{Co}) was calculated using the ImageJ software as A_i/A_{total}, where A_i and A_{total} are the total area values of Co nanoislands and the area of the STM image, respectively.

2.2. Sample preparation

Au single crystal was obtained from Mateck GmbH as a 10 mm diameter disc oriented in the (332) direction with surface roughness lower than 0.03 micron and orientation accuracy better than 0.1 degree. The surface was thoroughly cleaned prior to Co deposition using consecutive cycles of sputtering and annealing. Sputtering was performed using Ar^+ ions at 1 keV for shorts periods of time (typically 10–15 min) followed by annealing at ~750 K in order to regenerate the previously damaged surface. Annealing time typically ranged from 10 to 30 min. XPS measurements were performed between cycles to follow oxygen and carbon 1s photoelectron lines in order to ensure the effectiveness of the cleaning methodology. Once a clean state of the surface was achieved STM and LEED measurements were performed and Co was deposited from the tip of a Co wire at constant rate. Deposition time was varied in order to obtain different coverage. Deposits were investigated using XPS and STM. Finally, nitric oxide was injected in the preparation chamber in order to study the adsorptive properties of Co nanostructures. The partial pressure of NO was 10^{-8} mbar and adsorption time was set to 8 min (4.8 Langmuir). After NO adsorption, the sample was immediately transferred to STM chamber for surface microscopy characterization. Both deposition and NO dosing were performed at 294 K (room temperature). After STM, XPS analysis was performed in order to verify potential modifications on the electronic properties of the sample.

3. Results and discussion

3.1. Clean Au(332) surface

As a first step, it is important to characterize the clean Au(332) substrate before Co deposition, in order to identify possible modifications of the surface as a consequence of Co nucleation. STM images showing the topography of clean Au(332) surface are shown in Fig. 1.

As can be seen from Figs. 1a and b, monoatomic steps are imaged as continuous and parallel rows oriented in a given direction. At high magnifications, where atomic resolution is achieved, the characteristic atomic arrangement of the 111 surface plane is clearly visible on terraces, as indicated by the lattice depicted in Fig. 1d. This is consistent with the expected atomic arrangement of the 332 face of Au since this surface belongs to the $[n(111) \times (110)]$ family of planes, in our case $n = 5$. Also, Fig. 1c confirms the stepped nature of the vicinal surface when 3D rendering of a 2D image is applied. Topographic profiles obtained from STM images with atomic resolution are shown in Fig. 2a and b. Mean values of terrace width and Au–Au bond distance were determined as 13.6 ± 0.1 Å and 2.71 ± 0.08 Å, respectively (theoretical values are 13.32 Å and 2.88 Å for the hard sphere model of a stepped surface of such crystallographic orientation proposed by Clavilier et al. [15], using a lattice parameter of 4.08 Å). The differences observed between the theoretically calculated value and the value measured from STM images of terrace width could be explained by the relaxations of the topmost atomic layers compared to bulk positions and to the elastic interactions between steps as determined by Prévot et al. [16]. Nevertheless, the discrepancy between d_{Au-Au} values (experimental vs. calculated) may be related to experimental error.

The clean and ordered state of the surface is evident as can be inferred from STM pictures and supported by XPS and LEED pattern. The absence of C1s and O1s photoelectron lines in XPS spectrum in Fig. 2c suggests that the cleaning procedure of the sputtering/annealing cycling has successfully removed surface impurities. Consistently, LEED pattern of clean Au(332) surface in Fig. 2d displays well-defined spots revealing long-range ordering of the surface, which is in agreement with results reported in the literature by various authors for crystals of the same family of planes (see e.g. ref. [17]). For instance, the resulting pattern consists of the regular three-fold symmetry spots of the (111) face with satellite spots regularly spaced from the main spots. These secondary or satellite spots are generated by the periodic nature of the steps all over the surface. From LEED pattern shown in Fig. 2d, the ratio $d_{AuAu}/w_{terrace}$ in the reciprocal space was calculated. When we compare this value with the expected one calculated from values found in the literature we conclude, without any doubt, that the surface orientation is (332). Thus, having established the initial state of the substrate, Co nanostructures were deposited and results on its characterization are addressed in the following section.

3.2. Co deposition on vicinal Au

STM images show that Co deposition seems to be homogeneous on Au(332) at least in the coverage range investigated. Moreover, the deposition of the Co does not modify the structure of steps on the underlying substrate; since parallel rows clearly visible on the clean surface remain unchanged after Co deposition (e.g. see Figs. 3a and b). Moreover, the nearly random nature of nucleation and growth of Co nanostructures is confirmed compared to the Au(788) surface [13].

On the other hand, analyzing the heights of the bright spots of Co/Au(332) samples from the two topographic profiles presented in Fig. 3d, we find values around 2.2 and 4.2 Å for deposits having θ_{Co} of 0.17 and 0.64, respectively. Considering the values reported in the literature [9] of 2.05 Å and 4.1 Å for a mono and bilayer of Co(0001) on Au(111), respectively, we conclude that Co deposition on Au(332) occurs via island formation with maximum average height of a bilayer of Co atoms for the highest coverage investigated. In the case of the sample

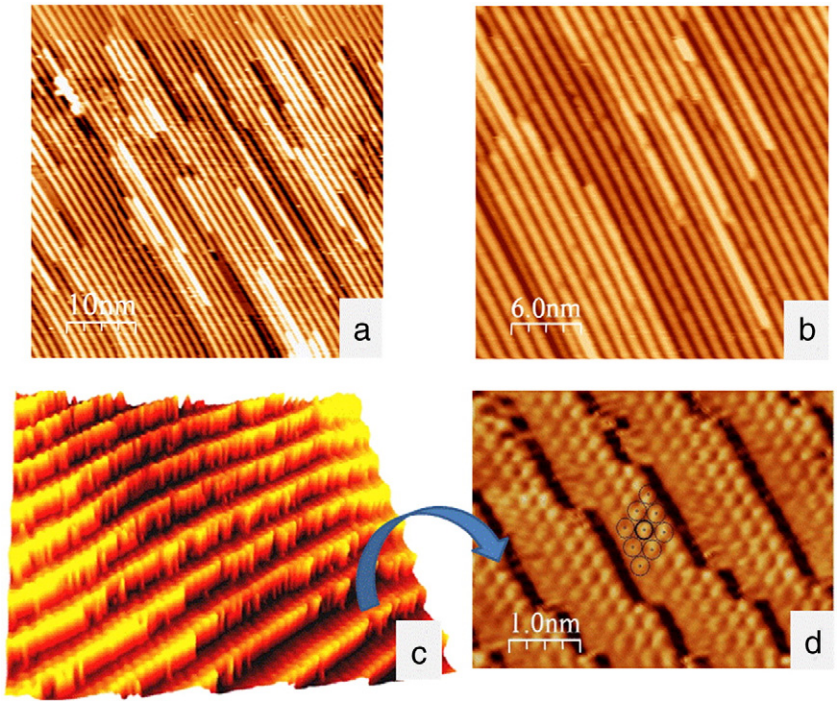

Fig. 1. STM images of clean Au(332) surface at different magnifications showing the periodic stepped nature of the surface (a–c) and the atomic arrangement at terraces (d). Tunneling conditions: a, b) $I_t = 0.17$ nA, $V_{bias} = 1.5$ V; c) $I_t = 0.3$ nA, $V_{bias} = 1.7$ V and d) $I_t = 0.3$ nA, $V_{bias} = 1.75$ V.

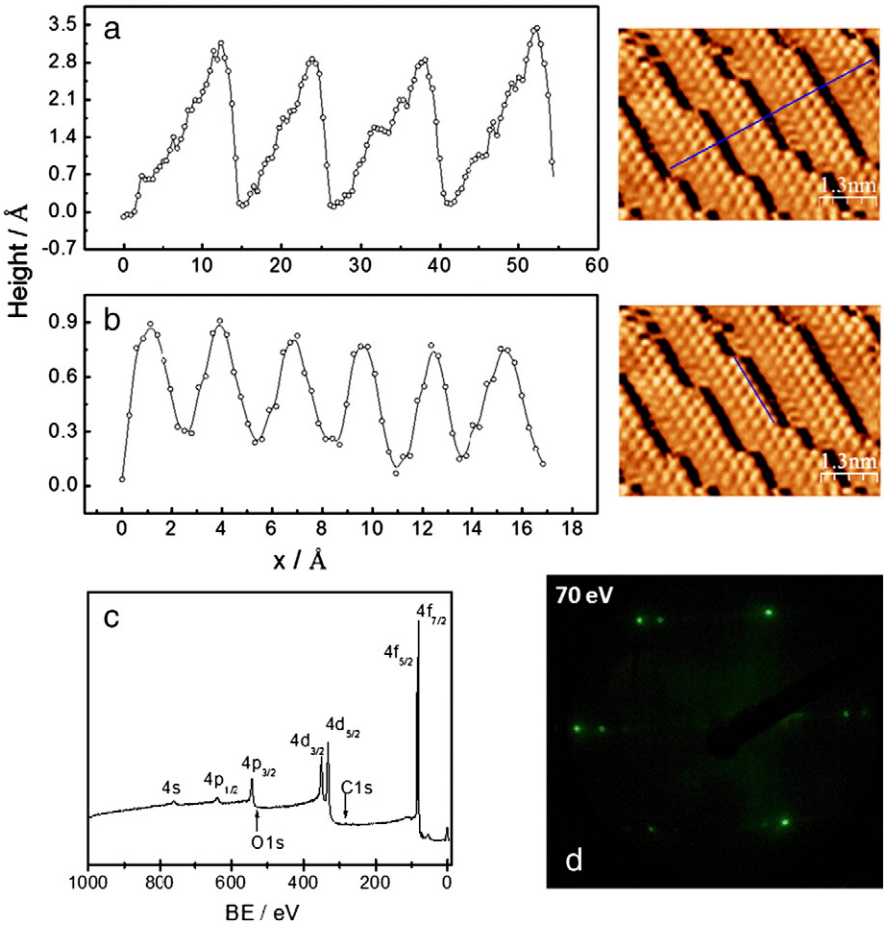

Fig. 2. Topographic profile lines obtained from STM images. (a) Profile across the monoatomic steps, (b) profile across a line of atoms at step/edge. (c) Survey XPS scan and (d) LEED pattern of clean Au (332).

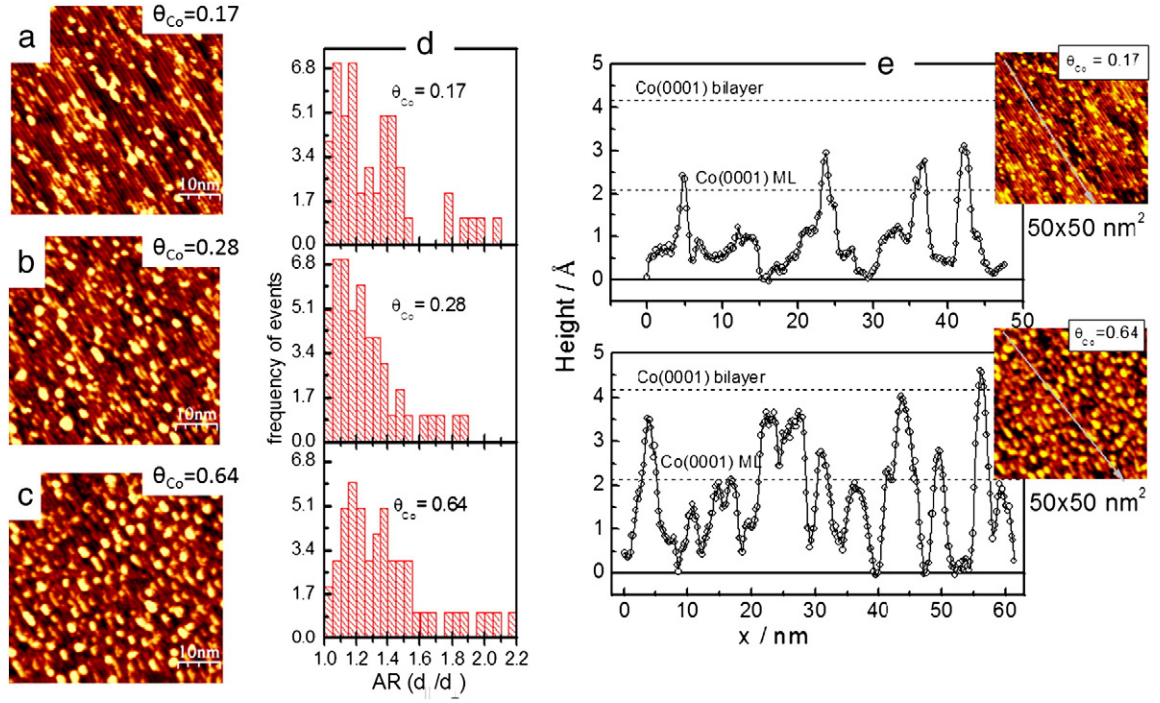

Fig. 3. (a–c) STM images of Co/Au(332) surfaces for different θ_{Co} as indicated. (d) Histograms showing aspect ratio (AR) distribution of Co islands and (e) topographic profiles of Co nanoislands calculated from STM image presented in the insets for $\theta_{Co} = 0.17$ and 0.64, as indicated. Tunneling conditions: a) $I_t = 0.28$ nA, $V_{bias} = 1.2$ V; b) $I_t = 0.24$ nA, $V_{bias} = 1.49$ V and c) $I_t = 0.28$ nA, $V_{bias} = 1.25$ V.

having $\theta_{Co} = 0.64$, the bilayer islands seem to coexist with islands having a monolayer height, suggesting a typical 3D island growth. Manual counting of island heights performed for the lowest and the highest coverage investigated reveals that in the case of $\theta_{Co} = 0.17$; 98% of Co islands are monolayers, while in the case of $\theta_{Co} = 0.64$; 51% of islands are bilayers of Co.

Additionally, a series of histograms are shown in Fig. 3d for the three Co/Au(332) surfaces investigated showing aspect ratio (AR) distribution of the islands. As can be seen from the histograms, at the highest coverage the frequency of events at large AR values increases, although at the low AR there is still a large number of events, suggesting that a high number of islands is nearly circular (with AR approaching to 1). However, the relatively high number of events in the region $1.2 < AR < 2.2$ for all samples suggests that substrate induces an anisotropic growth of Co nanoislands. Since AR values were calculated as the ratio ($d_{||}/d_{\perp}$) with $d_{||}$ and $d_{\perp}$ being the island diameter in the direction parallel and perpendicular to the steps, respectively, we conclude that the preferential growth of Co islands occurs in the direction parallel to the steps ($d_{||} > d_{\perp}$).

Electronic properties of the Co nanoislands can be qualitatively assessed analyzing the core-level photoelectron spectra of the Co 2p lines for all samples. Spectra collected are shown in Fig. 4. Firstly, a consistent increase in Co2p3/2 line intensity is clearly observed relative to Au 4s line at ca. 761.7 eV as deposition time increases. For all Co/Au(332) samples the Co2p3/2 photoelectron line is centered at binding energy (BE) 778 eV indicating that Co is present in the Co° chemical state. By comparing the line shape of this photoemission line with spectra reported in the literature for various Co-containing compounds [18], the absence of well-known satellites in photoelectron spectra of Co^{n+} species is in agreement with the metallic nature of Co nanoislands.

Moreover, the fact that the BE of the Co $2p_{3/2}$ line is equal to that in bulk Co would suggest that alloy formation, if there is any, takes place at the Co–Au interface to a minor extent under the experimental conditions used for deposition, since once the alloy is formed a shift in core level BE (core-level shift, CLS) is expected. Just to provide a reference, bimetallic systems similar to Co–Au such as Ni–Pt and Ni–Au exhibit CLS in the range from −0.4 to −0.7 eV for Ni 2p lines according to Steiner et al. [19]. The lack of alloy formation was also suggested in various papers regarding the study of the valence band structure on the Co/Au(111) system using ultra-violet photoelectron spectroscopy (UPS). [8]. In those cases, the authors ruled out Co–Au alloy formation since BE of Au $5d_{5/2}$ valence band states remains unchanged after Co deposition on Au(111). However, the appearance of a completely new feature in UPS spectra is assigned to a not well understood strong interaction between Co and Au.

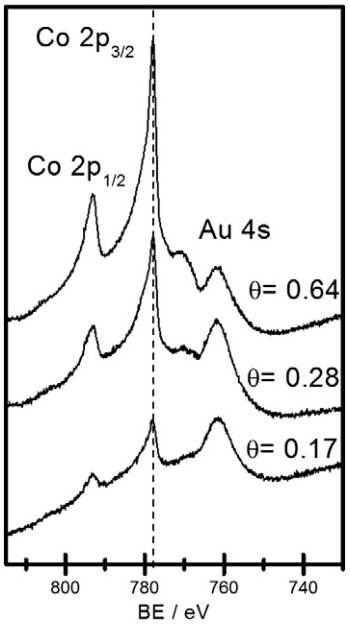

Fig. 4. X-ray photoelectron spectra of Co 2p photoemission lines for different θ_{Co} as indicated.

In order to investigate the stability of the Co nanoislands, Co-modified substrate was submitted to thermal annealing up to 590 K for 600 s. The resulting STM images for $\theta_{Co} = 0.17$ and 0.64 recorded after annealing are shown in Fig. 5. For the $\theta_{Co} = 0.17$, a series of black spots appear after the annealing treatment, and the structures visible in Fig. 3 before annealing are no longer visible after heat treatment. It is worth mentioning at this point that C and O contamination was not detected by XPS.

In contrast, in the case of $\theta_{Co} = 0.64$, some islands are still visible after heating, although most of the features disappear. Considering the results published by Ruban et al. [20], regarding the calculation of surface segregation energies in transition metal alloys, in the Co–Au system (provided that Au is the host element and Co the solute) a strong anti-segregation is predicted by their theory. Furthermore, thermodynamics tells that in the case of a binary alloy the surface concentration of the element having the lowest $\Delta H_{sublimation}$ (in this case Au) will be higher, provided that the driving force for segregation is the difference in the bonding energies between the components in the alloy and its influence in the surface tension relative to the pure constituents (see ref. [21] for more details). Thus, a migration of Co atoms into the bulk is expected to occur upon annealing. Cobalt migration into underlying atomic layers of Au(332) crystal should be responsible for the appearance of black spots observed by STM for the $\theta = 0.17$. In the case of the $\theta = 0.64$ there are also black spots, although its surface concentration seem to be smaller. Additionally STM images obtained for this deposit show that some Co structures remains at the surface and their dimension are much higher than for the unannealed sample (compare Fig. 3c with Fig. 5c). More important, topographic profiles shown in Fig. 5d for line scans depicted in image 5c show that Co islands height remains unchanged (as in the case of Fig. 3f) although island diameter increases, indicating that, in addition Co migration into Au, island tends to coalesce due to temperature rise.

Nevertheless, the depth of Co diffusion into the Au bulk cannot be directly assessed with STM images. Thus, photoelectron spectra were collected after annealing and the result for $\theta = 0.17$ deposit is shown in Fig. 6e (spectrum II). Comparing spectra I and II in Fig. 6e it is possible to note that the intensity of Co $2p_{3/2}$ photoelectron line relative to Au 4s line decreases after annealing, implying that surface concentration of Co has decreased upon annealing; thus, Co atoms initially at the surface diffuse into the substrate.

STM images similar to those presented in Fig. 5a and b, but for the basal planes of Au have already been reported in the literature for other systems [22]. In that case dark spots observed were ascribed to Pt insertion into Au lattice due to alloying, with and apparent "hole" depth of 0.2 Å. In our case, dark spots due to Co insertion are caused by the annealing, giving an apparent depth of 1.5 Å. Since we believe that differences in apparent depth due to electronic factors are relatively small compared to differences due to true depressions on the surface we believe that black spots are true geometric features where Co insertion took place after annealing. This idea of Co insertion is also supported by our XPS results, as mentioned earlier.

Regarding the electronic properties of the modified surface after annealing, XPS data in Fig. 6e (spectrum II) shows that, even after annealing, Co 2p line BE remains unchanged, a fact that has at least 2 implications: i) Co atoms retain the same chemical state before the annealing (Co°) and ii) even after annealing alloy formation is not detected by chemical shifts. From the last observation we could infer that even although Co atoms diffuse into Au, they might agglomerate

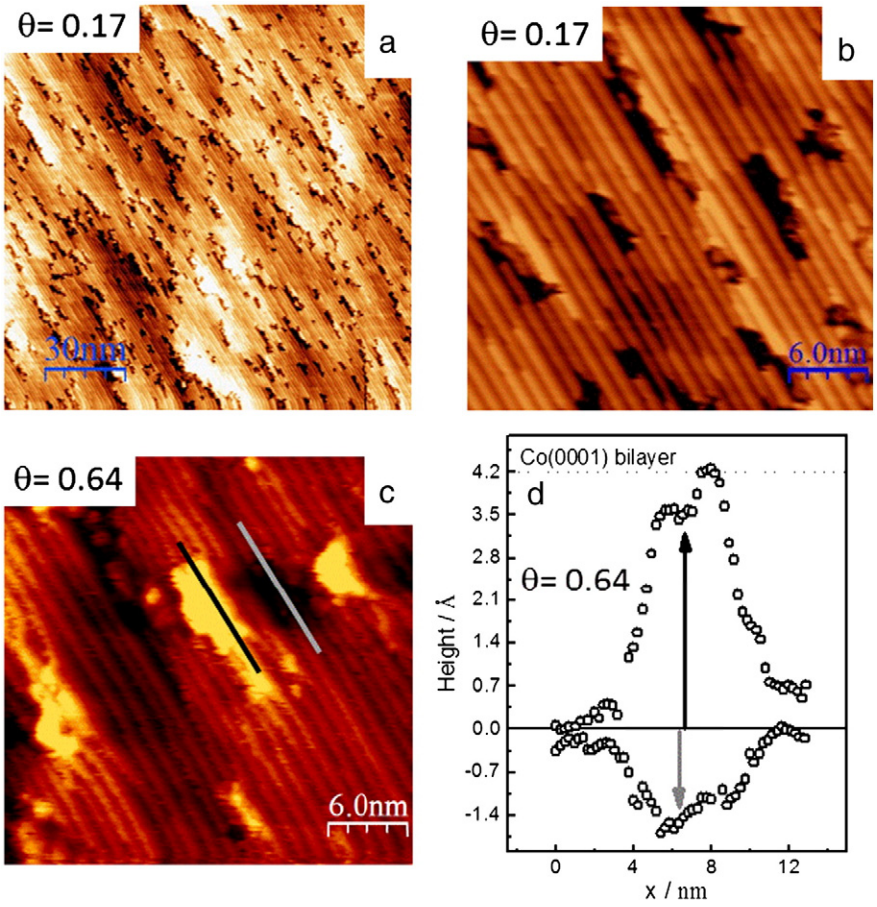

Fig. 5. STM images showing surface state after annealing of Co/Au(332) samples having $\theta = 0.17$ (a,b) and $\theta = 0.64$ (c). Topographic line profile of features identified in (c) is presented in (d). Tunneling conditions: a) $I_t = 0.5$ nA, $V_{bias} = 1.72$ V; b) $I_t = 0.18$ nA, $V_{bias} = 1.25$ V and c) $I_t = 0.24$ nA, $V_{bias} = 1.45$ V.

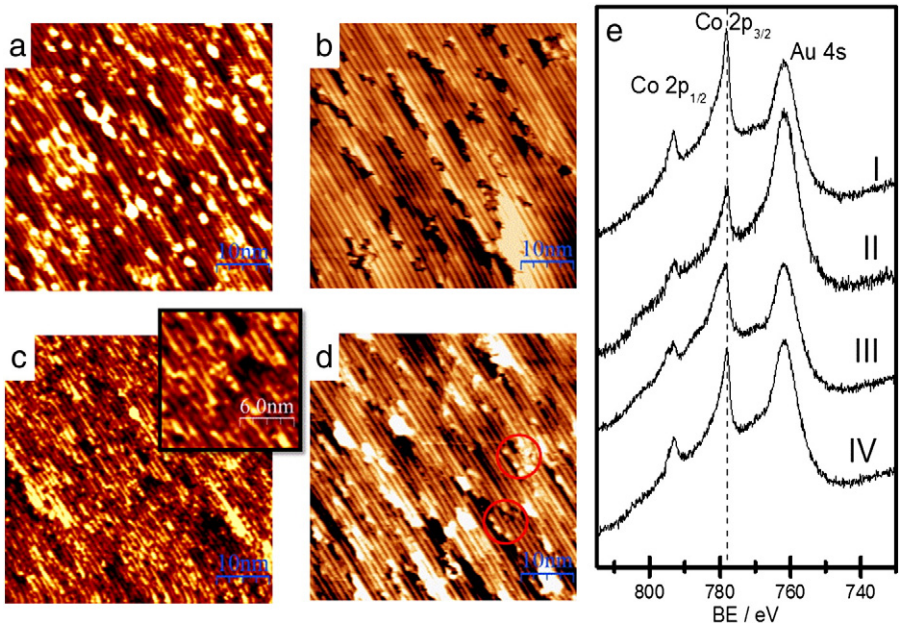

Fig. 6. (a) and (b) correspond to STM images for as prepared and annealed Co/Au(332), respectively. STM images in (c) and (d) correspond to as prepared and annealed NO/Co/Au(332) sample, respectively. (e) Spectra series of Co 2p core level lines for: I- Co/Au(332) as prepared, II- annealed Co/Au(332), III- NO/Co/Au(332) and IV- annealed NO/Co/Au(332). Tunneling conditions: a) $I_t = 0.28$ nA, $V_{bias} = 1.2$ V; b) $I_t = 0.18$ nA, $V_{bias} = 1.25$ V; c) $I_t = 0.33$ nA, $V_{bias} = 1.5$ V and d) $I_t = 0.32$ nA, $V_{bias} = 1.24$ V.

inside Au crystal in order to maximize the number of Co–Co interactions, otherwise chemical shifts should be expected due to dilution.

To further explore the stability of Co nanostructures, nitric oxide was adsorbed from gas phase and then, the NO/Co/Au(332) sample was submitted to the same thermal treatment mentioned earlier, using STM/XPS to follow the changes in morphology and chemical states. STM images of the resulting NO/Co/Au(332) surface before and after annealing are shown in Fig. 6c and d, respectively. It is possible to see that NO adsorption dramatically changes the structure of the Co nanoislands (compare Fig. 6c and a). For instance, the features of Co nanoislands clearly visible before NO adsorption are no longer present after NO exposure.

On the other hand Co 2p photoemission spectra of NO/Co/Au(332) before and after annealing are shown in Fig. 6e (spectra III and IV). XPS spectra reveal that at least one additional contribution and hence an additional chemical state of Co emerge upon NO adsorption (see spectrum III). At this point it is worth to mention that, based on STM/XPS measurements, NO adsorption on clean Au(332) is discarded since no additional features in the STM image and no O and N 1 s photoemission lines are observed (not presented here). These observations are in good agreement with results of Vinod et al. [23], who have demonstrated using the TPD technique that above 300 K NO completely desorbs from Au(310).

When NO/Co/Au(332) surface is submitted to thermal treatment, one could expect that NO molecules desorb from the surface following a dissociative path generating O and N adatoms or that the adsorption is dissociative itself, as demonstrated for Co(0001) by Bridge and Lambert using TPD and for Co(1010) by Gu et al. [24] using LEED, TPD and RAIRS. NO adsorption on transition metals has proven to be quite complex as can be appreciated in the review of Brown and King [25]. The dissociative vs. molecular adsorption paths strongly depend on the temperature at which adsorption occurs and the coverage of NO_{ads}. In the specific case of Gu et al., authors have determined that dissociative adsorption of NO is particularly important when dosing occurs at 300 K. In this way, comparing our XPS data for NO/Co/Au(332) with the all the exposed before, we suggest that the additional chemical state observed in spectrum III may be due to Co bonded to O adatom after dissociation of NO, since dissociative adsorption seems to be a reasonable scenario on Co nanoislands.

On the other hand, XPS data of the annealed NO/Co/Au(332) surface is shown in Fig. 6e (spectrum IV). Comparing spectra III and IV, it is possible to see that the additional contribution to the $2p_{3/2}$ line of Co at higher BE that emerged after NO adsorption disappears upon annealing. Thus, after desorption Co° seems to be the main phase present and the contributions associated with Co^{n+} species seem to vanish. More interestingly, comparing spectra II and IV, is possible to conclude that antisegregation of Co atoms occurs to some extent due to annealing, although the magnitude of Co 2p in spectrum IV is clearly higher than in absence of adsorbed NO (see spectrum II). These results are confirmed with STM measurements as can be seen in Fig. 6d, where STM image of annealed NO/Co/Au(332) is shown. For instance, bright spots (protrusions) such as those observed in Fig. 6a coexist on the surface with shadowed regions (depressions) as in Fig. 6b (red circles).

Finally, a closer look at the image of Fig. 6d suggests that the topography of annealed NO/Co/Au(332) ($\theta = 0.17$) is similar to that observed for annealed Co/Au(332) with $\theta_{Co} = 0.64$, having protrusions and shadowed areas coexisting in the same region of the surface. This, together with the fact that XPS intensity of Co 2p line does not decrease below Au 4s line as in the case of spectrum II of Fig. 6e, indicates that after NO molecule reacts with Co, there is a stabilization of the islands at the surface of Au(332) preventing Co diffusion into the substrate for the annealing conditions used.

4. Conclusions

Scanning tunneling microscopy reveals a well-ordered structure of the Au(332) surface with the expected values for terrace width and step height, confirming the typical hcp atomic arrangement of the 111 plane in the terrace. This surface is interesting because it provides a template to control size distribution of metallic NPs. In the present study we found that Co deposition occurs via nanoisland formation having mono or bilayer height. For instance, at higher coverage Co bilayers were found, although at lower coverage islands with almost only monoatomic height were observed. Regarding electronic properties of Co islands there is no evidence from XPS BE of alloy formation for all θ_{Co}, even after annealing of the sample. Upon NO adsorption a partial oxidation of Co was observed as indicated by the changes in line-

shape of Co 2p core line. XPS also shows that when submitted to thermal treatment, Co atoms diffuse into Au substrate leading to a loose of the structures originally visible in the STM images, although this diffusing effect is minimized when Co/Au(332) surface is exposed to NO.

Acknowledgments

Authors would like to thank Conselho Nacional de Pesquisa (CNPq) and Fundação de Amparo à Pesquisa do Estado de São Paulo (FAPESP) for financial support. Special thanks to L. H. Lima for discussions during STM measurements and Prof. G. Tremiliosi-Filho for lending the Au crystal. MJP thanks FAPESP for the fellowship granted (Proc. 2011/12.566-3). EAC thanks CNPq for the fellowship granted (Proc. 160172/2011-0).

References

[1] Metal Nanoparticles: Synthesis, Characterization, and Applications, CRC Press, 2001.
[2] J. Greeley, J.K. Norskov, M. Mavrikakis, Annu. Rev. Phys. Chem. 53 (2002) 319.
[3] Jinping Liu, Jian Jiang, Chuanwei Cheng, Hongxing Li, Jixuan Zhang, Hao Gong, Hong Jin Fan, Adv. Mater. 23 (18) (2011) 2076.
[4] R.C. Reed, The Superalloys: Fundamentals and Applications, Cambridge University Press, New York- USA, 2006;
J. Sato, T. Omori, K. Oikawa, I. Ohnuma, R. Kainuma, K. Ishida, Science 312 (5770) (2006) 90.
[5] Wu. Gang, Karren L. More, Christina M. Johnston, Piotr Zelenay, Science 332 (6028) (2011) 443.
[6] B.L.A. Shekoufeh, F. Lotfipour, Pharmazie 67 (10) (2012) 817.
[7] H. Wang, Y.F. Yu, Y.B. Sun, Q.W. Chen, Nano 6 (1) (2011) 1;
Hong-wang Zhang, Yi Liu, Shou-heng Sun, Front. Physiol. 5 (4) (2010) 347, (China).
[8] R. Mamy, Surf. Sci. 322 (1–3) (1995) 337;
R. Mamy, B. Carricaburu, J. Phys. Condens. Matter 5 (36) (1993) 6537.
[9] Bert Voigtländer, Gerhard Meyer, Nabil M. Amer, Phys. Rev. B 44 (18) (1991) 10354.
[10] Karina Morgenstern, Jakob Kibsgaard, Jeppe V. Lauritsen, Erik Lægsgaard, Flemming Besenbacher, Surf. Sci. 601 (9) (2007) 1967.
[11] S. Rousset, F. Pourmir, J.M. Berroir, J. Klein, J. Lecoeur, P. Hecquet, B. Salanon, Surf. Sci. 422 (1–3) (1999) 33.
[12] S. Rohart, G. Baudot, V. Repain, Y. Girard, S. Rousset, H. Bulou, C. Goyhenex, L. Proville, Surf. Sci. 559 (1) (2004) 47;
Y. Girard, G. Baudot, V. Repain, S. Rohart, S. Rousset, A. Coati, Y. Garreau, Phys. Rev. B 72 (15) (2005) 155434;
V. Repain, J.M. Berroir, S. Rousset, J. Lecoeur, Surf. Sci. 447 (1–3) (2000) L152.
[13] V. Repain, G. Baudot, H. Ellmer, S. Rousset, Europhys. Lett. 58 (5) (2002) 730.
[14] Caroline A. Schneider, Wayne S. Rasband, Kevin W. Eliceiri, Nat. Methods 9 (7) (2012);
I. Horcas, R. Fernandez, J.M. Gomez-Rodriguez, J. Colchero, J. Gomez-Herrero, A.M. Baro, Rev. Sci. Instrum. 78 (1) (2007) 013705.
[15] J. Clavilier, K. Elachi, A. Rodes, Chems. Phys. 141 (1) (1990) 1.
[16] G. Prévot, Y. Girard, V. Repain, S. Rousset, A. Coati, Y. Garreau, Jaita Paul, Nisha Mammen, Shobhana Narasimhan, Phys. Rev. B 81 (7) (2010) 075415.
[17] B. Lang, R.W. Joyner, G.A. Somorjai, Surf. Sci. 30 (2) (1972) 454.
[18] Mark C. Biesinger, Brad P. Payne, Andrew P. Grosvenor, Leo W.M. Lau, Andrea R. Gerson, Roger St C. Smart, Appl. Surf. Sci. 257 (7) (2011) 2717;
In: John F. Moulder, William F. Stickle, Peter E. Sobol, Kenneth D. Bomben (Eds.), Handbook of X Ray Photoelectron Spectroscopy: A Reference Book of Standard Spectra for Identification and Interpretation of XPS Data, Perkin-Elmer Coorporation, USA, 1995.
[19] P. Steiner, S. Hüfner, N. Mårtensson, B. Johansson, Solid State Commun. 37 (1) (1981) 73.
[20] A.V. Ruban, H.L. Skriver, J.K. Nørskov, Phys. Rev. B 59 (24) (1999) 15990.
[21] Michael Bowker, Chem. Vap. Deposition 1 (3) (1995) 90.
[22] P. Campiglio, V. Repain, C. Chacon, O. Fruchart, J. Lagoute, Y. Girard, S. Rousset, Surf. Sci. 605 (13–14) (2011) 1165.
[23] C.P. Vinod, J.W. Niemantsverdriet Hans, B.E. Nieuwenhuys, Appl. Catal. Gen. 291 (1–2) (2005) 93.
[24] J. Gu, Y.Y. Yeo, L. Mao, D.A. King, Surf. Sci. 464 (2–3) (2000) 68.
[25] Wendy A. Brown, David A. King, J. Phys. Chem. B 104 (12) (2000) 2578.